Semiclassical approach for path integrals in quantum mechanics

Author: Álvaro Peña Almazán
Facultat de Física, Universitat de Barcelona, Diagonal 645, 08028 Barcelona, Spain.

Advisor: Juan M. Torres
(Dated: June 13, 2023)

Abstract: In this work we have explored the formalism of the path integral in the semiclassical approximation and we have obtained both analytical and numerical results to determine the expected values of quantum observables incorporating thermal fluctuations. The study has been done for the harmonic and anharmonic potentials in one dimension. The obtained results have been compared with those obtained by solving the Schrödinger equation and the path integral Monte Carlo method; the similarities and discrepancies have been discussed.

I. INTRODUCTION

Richard P. Feynman, in 1948, was responsible for developing the path integral (PI) formulation of quantum mechanics (QM) that focuses on trajectories weighted by the action, and probability distributions as an alternative description to Schrödinger's wave function [1, 2].

When working in classical mechanics, out of all the possible paths that a system can take to go from one point (t_a, x_a) to another point (t_b, x_b), only one will have to be considered, we will call it $x_{cl}(t)$. This path will be the one satisfying *the principle of least action*, where the action for an arbitrary potential $V(x)$ is defined as,

$$S = \int_{t_a}^{t_b} dt \left[\frac{1}{2} m \left(\frac{dx}{dt} \right)^2 - V(x) \right] . \tag{1}$$

In the PI formalism of QM, the situation is significantly different. Not a unique path is relevant; we have to account for all of them. Therefore, we need to define a probability amplitude that will be the weighted sum of the contributions from all possible paths. We will call this amplitude the *kernel* and will be the main character of the QM approach we will explore in this work.

As time has passed, this revolutionary approach to QM has demonstrated its usefulness in handling non-perturbative interactions, in computing correlation functions and also has proven to be a fundamental tool in the development of quantum field theory.

The goal of this work is to introduce the PI formalism in QM within the semiclassical approximation and illustrate these concepts by performing analytical and numerical calculations for the harmonic oscillator (HO) and anharmonic oscillator (AHO) potentials.

II. PATH INTEGRAL: THEORETICAL DEVELOPMENT

A. Path integral formalism

The contributions to the probability amplitude of a particle traveling from the spacetime point a to point b have equal magnitudes but different phases. These phases are determined by the particle's action [3, 4],

$$\phi\left[x(t)\right] \propto e^{(i/\hbar)S[x(t)]} , \tag{2}$$

where $x(t)$ is the particle's trajectory, $S\left[x(t)\right]$ is the particle's action and $\hbar$ is the Planck's constant. Therefore, calling $K(b;a)$ the probability amplitude (kernel) from a to b:

$$K(b;a) = \sum_{paths} \phi\left[x(t)\right] . \tag{3}$$

To compute the sum over all the paths we draw an analogy with the Riemann sum. We build each path by discretizing the temporal variable into N steps of size ϵ. For each time step t_i we select a corresponding point x_i, then we connect all the points (t_i,x_i), (t_{i+1},x_{i+1}) using straight lines and integrate each x_i. Thus we will have:

$$K(b;a) \sim \int ... \int \int \phi\left[x(t)\right] dx_1 dx_2 ... dx_{N-1} . \tag{4}$$

The points $x_0 = x_a$ and $x_N = x_b$ are not included in the integration because they are fixed in our trajectory.

To express (4) more accurately we need to take the limit as $\epsilon \to 0$. To accomplish it we will introduce a convenient normalization factor, such that,

$$K(b;a) = \lim_{\epsilon \to 0} \frac{1}{A} \int \int ... \int e^{(i/\hbar)S[b,a]} \frac{dx_1}{A} \frac{dx_2}{A} ... \frac{dx_{N-1}}{A} , \tag{5}$$

where $A = \left(\frac{2\pi i\hbar\epsilon}{m}\right)^{1/2}$ and (2) has been employed as well.

Usually, we will express the above equation in terms of $\mathcal{D}x$ which represents the integral over all possible paths,

$$K(b;a) = \int_{x_a}^{x_b} \mathcal{D}x \; e^{(i/\hbar)S[x(t)]} . \tag{6}$$

As we mentioned earlier, the kernel will be an amplitude, consequently, we can see the kernel as a probability distribution. Another common way of expressing the kernel in QM will be the so-called spectral representation [1],

$$K(x_b, t_b; x_a, t_a) = \sum_n \phi_n(x_b)\phi_n^*(x_a)e^{(-i/\hbar)E_n(t_b-t_a)} \ , \tag{7}$$

where $\phi_n(x)$ and E_n are respectively the eigenfunction and eigenvalue of the n-th energy state, solution of the Schrödinger equation with the corresponding potential.

As will be discussed later, we are only interested in closed paths, therefore, we will take $x_a = x_b = x$, and without loss of generality, $t_a = 0$ and $t_b = t$ also will be taken. Hence,

$$K(x, t; x, 0) = \sum_n |\phi_n(x)|^2 e^{-iE_n t/\hbar} \ . \tag{8}$$

B. Finite temperature

We observe a similarity between the exponential term in the equation (8) and the partition function [1],

$$\mathcal{Z}(\beta) = \sum_n e^{-\beta E_n} \ , \tag{9}$$

where $\beta = 1/(k_B T)$. Furthermore, if we examine the expression for the density matrix of a system [1],

$$\rho(x', x) = \sum_n \phi_n(x')\phi_n^*(x)e^{-\beta E_n} \ , \tag{10}$$

we note that is remarkably similar to the kernel definition shown in Eq. (7). In fact, we can identify both expressions if we impose,

$$it = \hbar\beta \ . \tag{11}$$

Therefore we will define a new imaginary time $\tau = it = \hbar\beta$ ($\tau_a = it_a$, $\tau_b = it_b$) through which we can incorporate the temperature. From now on we will lose the notion of real time, the new imaginary time cannot be easily interpreted as the standard time anymore. Moreover, this will have relevant effects on our calculations of the kernel, as we will see later on.

For an arbitrary potential $V(x)$, the standard action will be the one shown in Eq. (1), but applying the redefinition mentioned in Eq. (11) we obtain,

$$S = i\int_{\tau_a}^{\tau_b} d\tau \left[\frac{1}{2}m\left(\frac{dx}{d\tau}\right)^2 + V(x)\right] = iS_E[x(\tau)] \ , \tag{12}$$

where the Euclidean action, S_E, has been identified. We can now introduce this into the PI expression (Eq. (6)), resulting in,

$$K(x_b, \tau_b; x_a, \tau_a) = \int_{x_a}^{x_b} \mathcal{D}x \ e^{-S_E[x(\tau)]/\hbar} \ . \tag{13}$$

By obtaining an exponential with a real quantity, we can now interpret it as a statistical weight instead of a phase, as we had done previously when dealing with an imaginary exponent. Since we are interested in computing expected values of some operators depending on the position, we will consider only diagonal elements of the density matrix. Therefore we take $x_b = x_a \equiv x_o$ which we will call the observation point. Without loss of generality, we will also take $\tau_a = 0$, $\tau_b = \tau$, using (11) we will have $\tau = \hbar\beta$.

To compute the Euclidean action we will use the semiclassical approximation in which we make an expansion around the classical trajectory. In this approximation, we will consider that the largest contribution to the PI is due to the classical trajectory and the paths around it [2], then,

$$x(\tau) = x_{fl}(\tau) + y(\tau) \ . \tag{14}$$

The classical trajectory that moves from point (0, x_o) to ($\hbar\beta$, x_o) will be called flucton, and it will satisfy the Euler-Lagrange equations [5]. The flucton corresponds to the first term in the previous equation, while the second term represents fluctuations around it.

We will have,

$$S_E[x(\tau)] = S_E[x_{fl}(\tau) + y(\tau)] \ . \tag{15}$$

Thus, we can perform an expansion of S_E,

$$S_E[x(\tau)] = S_{cl} + \int d\tau \left.\frac{\delta S_E}{\delta x(\tau)}\right|_{x_{fl}} y(\tau) + \frac{1}{2}\int d\tau \int d\tau' \left.\frac{\delta^2 S_E}{\delta x(\tau)\delta x(\tau')}\right|_{x_{fl}} y(\tau)y(\tau') + ... \ , \tag{16}$$

which is the series expansion for a functional. We will start calculating the S_{cl}, which is the classical action. Clearly, $S_{cl} = S_E[x_{fl}(\tau)]$, so we will need to calculate the expression of $x_{fl}(\tau)$ to compute the classical action.

Harmonic oscillator

We first consider the 1D HO potential that has the form,

$$V(x) = \frac{1}{2}m\omega^2 x^2 \ , \tag{17}$$

where m is the particle's mass, ω is the frequency of the potential and x is the particle's position. Using the classical equations of motion:

$$m\ddot{x}(\tau) - m\omega^2 x(\tau) = 0 \ . \tag{18}$$

This equation can be solved analytically with the following boundary conditions,

$$x(\tau = 0) = x_o \qquad x(\tau = \hbar\beta) = x_o \ , \tag{19}$$

we find,

$$x_{fl}(\tau) = \frac{x_o}{\exp(\omega\hbar\beta) + 1}\left[\exp(\omega(\hbar\beta - \tau)) + \exp(\omega\tau)\right] \ . \tag{20}$$

Thus,

$$S_{cl} = \int_0^{\hbar\beta} d\tau \frac{m\omega^2 x_o^2}{(e^{\omega\hbar\beta}+1)^2}\left[e^{2\omega\tau}+e^{2\omega(\hbar\beta-\tau)}\right] = \\ = m\omega x_o^2 \frac{e^{\hbar\beta\omega}-1}{e^{\hbar\beta\omega}-1} = m\omega x_o^2 \tanh\frac{\hbar\beta\omega}{2} \ . \quad (21)$$

We have obtained the expression for the classical action (first term of the semi-classical expansion).

We know that the first-order fluctuation (second term in Eq. (16)) must be zero because the *principle of least action* demands $\delta S_{cl} = \delta S_E/\delta x(\tau)|_{x_{fl}} = 0$.

For the HO potential, the expansion of the action in Eq. (16) ends with the quadratic term, and higher-order terms become zero. Moreover, the quadratic term becomes a constant, and therefore, there is no need to compute it as it can eventually be fixed by the normalization of the probability. In conclusion, for the HO potential, we can calculate the exact kernel using only (21),

$$K(x_o, \hbar\beta; x_o, 0) = e^{-\frac{m\omega x_o^2}{\hbar}\tanh\frac{\hbar\beta\omega}{2}} \ . \quad (22)$$

This solution coming from the flucton path (when normalized) matches the well-known exact solution for the HO, appearing for example in Ref. [1].

Anharmonic oscillator

In the previous section, we have been able to take into account the fluctuations and compute an exact function of the kernel due to the quadratic dependence of the HO potential on the position. However, with the AHO oscillator, the situation becomes more complicated.

The anharmonic (quartic) potential will take the form,

$$V(x) = \frac{1}{2}m\omega^2 x^2 + \frac{1}{2}g^2 x^4 \ . \quad (23)$$

We will obtain the flucton (classical) solution numerically as described later. The first term of (16) will be again zero since $\delta S_{cl} = 0$, and the (space-dependent) higher-order terms will be not considered in this work, since they are much more complicated to address.

To validate the obtained results and estimate the systematic error introduced by neglecting the fluctuations in the semiclassical approximation we will compare them with the results obtained from the Schrödinger equation. This comparison will allow us to evaluate the accuracy of the approximation and quantify the discrepancies arising from neglecting the fluctuations. From (8) we know that

$$K(x_o, \hbar\beta; x_o, 0) = \sum_n |\phi_n(x)|^2 e^{-E_n\beta} \ . \quad (24)$$

We can calculate numerically the values of the wave functions and the energies through the Schrödinger equation and compute the sum. The details on how to perform this numerical calculation are given in the Appendix.

We will also compare the results obtained with those acquired from the Path Integral Monte Carlo method [6].

III. NUMERICAL CALCULATION AND RESULTS

From now on we will simplify notation, and call x for the observation point, instead of x_o. Additionally, for simplicity, we will choose units such that $\hbar = k_B = 1$ and also set $\omega = m = 1$.

The problem we aim to solve is to find the first term of the semiclassical expansion Eq. (16) of the PI in QM. Numerically this can be reduced to a boundary value problem, which means we must solve $x_{fl}(\tau)$, solution of the second-order differential equation,

$$\ddot{x}(\tau) - V'(x) = 0 \ , \quad (25)$$

with Dirichlet-type boundary conditions, which are shown in Eq. (19).

Since we have Dirichlet boundary conditions, we will make use of the function *scipy.integrate.solve_bvp* from the SciPy module. This function implements a fourth-order collocation method solved through a Newton method. The collocation method involves discretizing the solution domain and approximating the solution at those points. Then, an optimization problem is formulated to minimize the difference between the solution and the boundary conditions. The Newton method will be used to iteratively update the collocation points and approach a solution that satisfies the imposed conditions.

Once we have obtained the kernel numerically, we will be able to calculate the expected values of any observable which depend on x, $\mathcal{A}(x)$, using

$$\langle\mathcal{A}\rangle = \int_{-\infty}^{\infty} \mathcal{A}(x)P(x)dx \ , \ P(x) = \frac{K(x,\hbar\beta;x,0)}{\int_{-\infty}^{\infty} K(x,\hbar\beta;x,0)dx} \ , \quad (26)$$

where $K(x, \hbar\beta; x, 0) = \exp\left(-S[x_{fl}(x)]\right)$.

A. Harmonic oscillator

We will first show the flucton trajectory $x_{fl}(\tau)$ and the probability distribution that we have obtained by numerically solving the Eq. (25).

Figure 1 presents the numerically computed flucton for the HO potential, obtained by solving Eq. (18), depicted as a blue solid line. Additionally, the exact solution given by Eq. (20) is shown as solid circles. We obtain an excellent agreement between both solutions.

In Figure 2 we show in blue solid line, red dashed line, and green dash-dotted line the numerically computed probability for the HO for $\beta = 10.0$, $\beta = 1.0$, and $\beta = 0.1$ respectively. In addition, the exact probability given by Eq. (22) normalized has been shown in the three different temperatures by circles, crosses and diamonds, respectively. The discrepancy between the exact result and the numerical flucton is negligible. Thus we can ensure that the numerical method is pretty accurate. At low temperatures, thermal fluctuations are negligible,

and the probability distribution will coincide with the square of the ground state wave function. As the temperature increases, we can observe how the probability distribution broadens due to the growing population of excited states caused by thermal fluctuations.

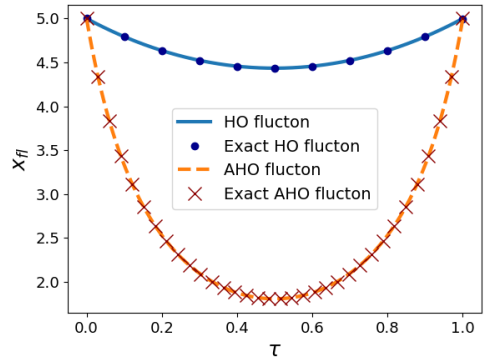

FIG. 1: Flucton path for the HO and AHO ($g = 1.0$) for $\beta = 1.0$ and $x_0 = 5$ compared with the exact solution and the analytic expression in Eq. (20), respectively.

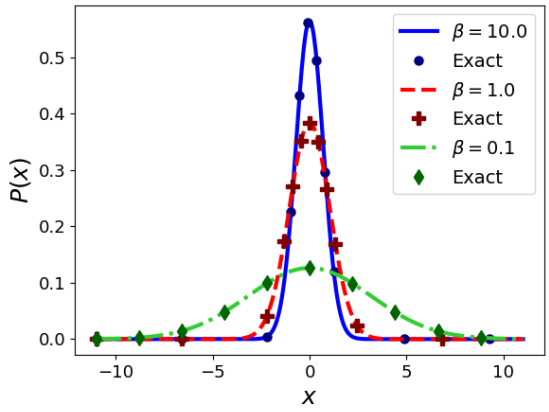

FIG. 2: Probability distribution of the HO for $\beta = 10.0$, $\beta = 1.0$, and $\beta = 0.1$ with their exact solutions from Eq. (22).

B. Anharmonic oscillator

As we observed in the previous section, we can find an exact analytical solution for the flucton path for the HO potential but not for the AHO one. However, to compare our numerical results of the flucton in the AHO, we will use the semi-analytical exact solution given in Ref. [7].

Figure 1 shows the trajectory of the flucton $x_{fl}(\tau)$ obtained from numerical simulation and the semi-analytical exact solution. Both results exhibit perfect agreement, proving again the accuracy of the numerical calculation.

We will also compare the results of $P(x)$ obtained through the numerical flucton with those calculated through the Schrödinger equation and the Path Integral Monte Carlo simulation. Since we only account for the classical solution and neglect the higher-order terms, a difference with respect to the exact results is expected.

In Fig. 3 we show in red solid line the results from the numerical flucton, and in green dashed line the ones from the Schrödinger equation compared to the outcome of the Monte Carlo simulation, shown in dark green dots.

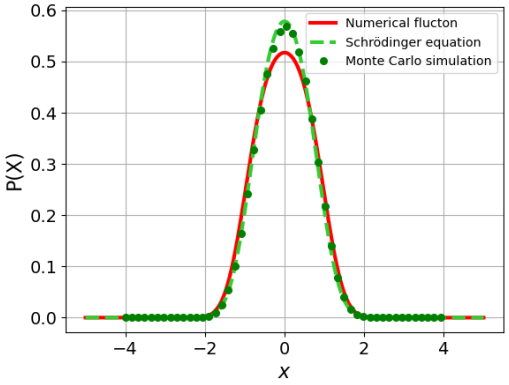

FIG. 3: Probability distribution in terms of the observation point for the AHO with $g = 1.0$ for $\beta = 1.0$.

In Fig. 4, we show the difference between the Schrödinger equation results and the numerical flucton using green solid, blue dashed, and red dash-dotted lines for $\beta = 10.0$, $\beta = 1.0$, and $\beta = 0.1$ respectively. We can observe discrepancies around $x = 0$, which would be reduced by introducing higher-order terms. However, the discrepancy is significantly reduced in the tails of $P(x)$, where the semiclassical approximation works better. On the other hand, the Monte Carlo and the Schrödinger results agree accurately, as expected.

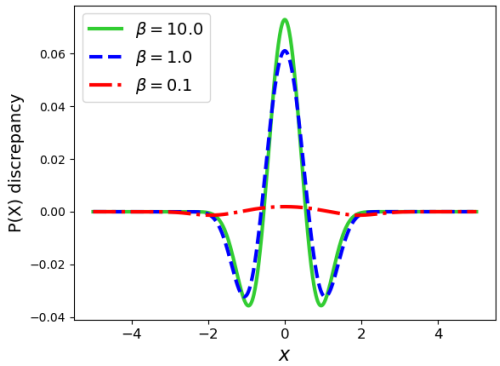

FIG. 4: Absolute difference between the results from the Schrödinger equation and the flucton ones (first term of the expansion (16)) for different temperatures ($T = 1/\beta$).

C. Energy Expectation values

Once we have made qualitative comparisons between all the methods used for calculating the probability distribution we will make a quantitative comparison through

the expected value of the energy $\langle E \rangle$.

From our $P(x)$ we can easily obtain expectation values of $x-$dependent quantities. To obtain $\langle E \rangle$ we will apply the virial theorem to connect the expected value of the energy to the expected values of different powers of x.

These expected values will be calculated using Eq. (26) where the integral goes from $-\infty$ to ∞. In practice, we will choose some large value of x to cut the integral, where we ensure that $P(x)$ is almost zero there.

The virial theorem states that for a potential of the form $V(x) = \alpha x^n$, it is fulfilled $2\langle T \rangle = n \langle V \rangle$.

We will have a generic potential like the one in Eq. (23) (the HO is obtained setting $g = 0$) thus,

$$\langle E \rangle = \langle x^2 \rangle + \frac{3}{2} g^2 \langle x^4 \rangle \ . \tag{27}$$

Using the expression (27) and the numerically computed values of $\langle x^n \rangle$ we will calculate $\langle E \rangle$.

	Numerical Flucton	Exact, Eq. (22)	Schrödinger Eq.
$\beta = 0.1$	10.0078347	10.0078348	10.003
$\beta = 1.0$	1.081981	1.081980	1.081977
$\beta = 10.0$	0.5005	0.500045	0.500040

TABLE I: Expected values of the energy of HO through each one of the methods ($g = 0$).

In Table I we can observe that the results obtained through the three different methods exhibit a very good agreement. Minor discrepancies can be attributed to discretization effects inherent to the numerical calculations.

	$\beta = 0.1$	$\beta = 1.0$	$\beta = 10.0$
Numerical flucton	8.010512	1.289979	0.8859
Exact flucton [7]	8.010510	1.289977	0.8860
Schrödinger equation	7.9047	1.0505	0.6962
Monte Carlo method	7.9841	1.1073	0.7369

TABLE II: Expected values of the energy of AHO through each one of the methods ($g = 1$).

In Table II we present the results for the AHO with $g = 1$, the results obtained through the numerical flucton and the exact flucton agree very well. Discrepancies can be attributed to discretization effects.

On the other hand, as was expected, the two results obtained through the flucton differ in a notable degree from the ones obtained through the Schrödinger equation and the Monte Carlo method. This discrepancy arises from neglecting higher-order terms in Eq. (16).

IV. CONCLUSIONS

In this work, we introduced the PI formalism and used the semiclassical approximation to numerically compute the probability distribution for both the HO and AHO potentials. We compared our results with those obtained from the Schrödinger equation and the Monte Carlo method.

For the HO potential, we obtained an exact analytical solution, Eq. (22), where fluctuations only contributed as an irrelevant constant prefactor. Our numerical simulation yielded satisfactory results, matching the analytical solution and the Schrödinger equation results (Table I).

For the AHO potential, for which we cannot obtain an exact and analytical solution of the kernel, our numerical simulation for the flucton has also perfectly matched with the exact flucton solution extracted from [7]. However, as expected, we found a discrepancy compared to the results obtained through the Schrödinger equation and Path Integral Monte Carlo simulation, due to neglecting the fluctuations in the calculation of the probability.

It would be highly interesting to further explore the investigation by incorporating higher-order terms in the semiclassical expansion (which would reduce the discrepancies found in the AHO case) and exploring additional potentials, such as the double well potential or even a two-body potential.

Acknowledgments

I would like to express my gratitude to my supervisor, Juan Torres, for his guidance and assistance throughout this work, as well as to Gerard Pons for his valuable support and permission to use his data. Lastly, I want to thank my family for their unwavering support in helping me achieve my goals.

[1] Richard P Feynman, Albert R Hibbs, and Daniel F Styer. *Quantum mechanics and path integrals*. Courier Corporation, 2010.

[2] Gert-Ludwig Ingold. Path integrals and their application to dissipative quantum systems. In *Coherent Evolution in Noisy Environments*, pages 1–28. Springer Berlin Heidelberg, 2002.

[3] R. Rosenfelder. Path Integrals in Quantum Physics, arXiv: 209.1315, 2017.

[4] Richard MacKenzie. Path Integral Methods and Applications, arXiv: quant-ph/0004090, 2000.

[5] M. A. Escobar-Ruiz, E. Shuryak, and A. V. Turbiner. Quantum and thermal fluctuations in quantum mechanics and field theories from a new version of semiclassical theory. *Physical Review D*, 93(10), may 2016.

[6] Gerard Pons Polo. Private communication, 2023.

[7] C.A.A. de Carvalho, R.M. Cavalcanti, E.S. Fraga, and S.E. Jorás. Semiclassical series at finite temperature. *Annals of Physics*, 273(1):146–170, apr 1999.

V. APPENDIX

A. Computing Schrödinger solutions

In order to compute the solution of the Schrödinger equation we will reduce the problem to an eigenvalue problem. We know that the Schrödinger equation in one dimension can be expressed as:

$$-\frac{\hbar^2}{2m}\frac{d^2}{dx^2}\phi_n(x) + V(x)\phi_n(x) = E_n\phi_n(x) \ , \qquad (28)$$

where the potential will be either the HO or the AHO. To compute the eigenvalues and eigenvectors we will build the left-hand side of the equation in matrix form (using finite differences for the first term) and solve the eigenvalue problem. This will allow us to obtain the eigenvalues, which correspond to the energies, along with the corresponding wave functions in terms of the position. Thus, we will be able to compare the resulting wave function with the value of the kernel previously found.

As β becomes smaller (T bigger) we will have states of larger values of n occupied (excited states), therefore we will need to compute more eigenvalues to approach correctly the solution. All calculations and figures presented have been made using $n = 100$ eigenvalues.

B. Numerical solution of Eq. (25)

To solve the differential equation given by Eq. (25), we used the Python function *scipy.integrate.solve_bvp* from the SciPy module. This function is specifically designed to solve boundary value problems using the collocation method in combination with the Newton method, as briefly described in Section III.

The function will require four inputs: two vectors and two functions. The first vector will be the discretized independent variable (in our case, imaginary time), and the second vector will be our initial guess for each time step of x and $\frac{dx}{d\tau}$, which we randomly initialize. The first function calculates the derivatives of x, taking a vector $\left[x, \frac{dx}{d\tau}\right]$ as input, and returning $\left[\frac{dx}{d\tau}, \frac{d^2x}{d\tau^2}\right]$. The last required function applies the boundary conditions and evaluates the difference between the obtained result and the specified boundary conditions.

We will need to execute this function in a loop, varying the values of the observation points x, in order to find the probability distribution.

Therefore, we have used a variable number of points for both the observation point values, denoted as N_x, and the time values, denoted as N_τ. For the calculations with $\beta = 10.0$, we have used $N_\tau = 10000$ and $N_x = 1000$ since in this case the probability distribution quickly approaches zero, requiring small values for the observation point ($x = 5$). We have determined that the execution under these conditions takes approximately 155 seconds.

On the other hand, for $\beta = 0.1$, we have performed the calculation with $N_\tau = 1000$ and $N_x = 10000$ as the value of β allows for a sufficiently low time step, enabling us to increase the resolution for the observation point, which is now larger ($x = 11$). Taking these values of N_τ and N_x the calculation is performed in approximately 120 seconds.

Given the fast execution and the high resolution achieved in the results, we did not need to further optimize the code. However, we could optimize the initial values we set for the *scipy.integrate.solve_bvp* function to potentially improve it.